THYROID
Volume 24, Number 4, 2014

DOI: 10.1089/thy.2013.0149

An *In Vivo* Mouse Model of Metastatic Human Thyroid Cancer

Lisa Zhang,[1] Kelli Gaskins,[1] Zhiya Yu,[2] Yin Xiong,[1] Maria J. Merino,[3] and Electron Kebebew[1]

Background: Mouse models of metastatic human cancers are important tools in preclinical studies for testing new systematic therapies and studying effectors of cancer metastasis. The major drawbacks of current mouse models for metastatic thyroid cancer are that they have low metastasis rates and do not allow *in vivo* tumor detection. Here, we report and characterize an *in vivo* detectable metastasis mouse model of human thyroid cancer using multiple thyroid cancer cell lines.

Methods: Human anaplastic thyroid cancer cell lines 8505C, C-643, SW-1736, and THJ-16T; follicular thyroid cancer cell lines FTC-133, FTC-236, and FTC-238; and Hürthle cell carcinoma cell line XTC-1 were transfected with a linearized pGL4.51[*luc2*/CMV/Neo] vector or transduced with lentivirus containing *Luc2*-eGFP reporter genes. The stably transfected cells were injected intravenously into NOD.Cg-*Prkdc*^{scid} *Il2rg*^{tm1Wjl}/SzJ mice. Tumors were detected with an *in vivo* imaging system—Xenogen IVIS. Vemurafenib, a BRAF inhibitor, was used to treat lung metastases generated from 8505C-*Luc2* cells with a *BRAF*^{V600E} mutation to test the accuracy of the model to evaluate response to therapy.

Results: Intravenous injection of as few as 30,000 8505C-*Luc2* cells produced lung metastases in 100% of the injected mice, and many of these mice also developed bone metastases at a later stage of the disease. Similarly, metastatic tumors also developed in all mice injected with C-643-*Luc2*, THJ-16T-*Luc2*, FTC-133-*Luc2*, FTC-236-*Luc2*, FTC-238-*Luc2*, and XTC-1-*Luc2* cells. The metastases were easily detectable *in vivo*, and tumor progression could be dynamically and accurately followed and correlated with the actual tumor burden. Furthermore, disease progression could be easily controlled by adjusting the number of injected cells. The *in vivo* treatment of 8505C xenograft lung metastases with vemurafenib dramatically reduced the growth and signal intensity with good correlation with actual tumor burden.

Conclusions: Herein we report an *in vivo* detectable mouse model of metastatic human thyroid cancer that is reliable and reproducible. It will serve as a useful tool in the preclinical testing of alternative systematic therapies for metastatic thyroid cancer, and for functional studies of thyroid cancer tumor biology *in vivo*.

Introduction

Thyroid cancer is one of the 10 most common cancer types in the United States, with increasing incidence and mortality rates (1). Thyroid cancer of follicular cell origin can be classified as well-differentiated, poorly differentiated, and anaplastic thyroid cancer. Well-differentiated thyroid cancer, including papillary and follicular thyroid carcinomas, is characterized by a slowly progressive course and a normally favorable prognosis. However, 10–15% of patients with differentiated thyroid cancer have aggressive disease and die from distant metastasis (2). The survival rate for patients with distant metastasis is approximately 57% (3). The most common metastasis site of thyroid cancer is the lung, followed by bone (2). About 15% of children and 10% of adults present with lung micrometastases at the time of the initial treatment (4). Anaplastic thyroid cancer is rare, accounting for 1% of all thyroid cancers (5). However, it is one of the most aggressive types of human malignancies, with a median overall survival of only six months from the time of diagnosis (6,7).

Although distant metastasis is responsible for most thyroid cancer morbidity and mortality, mouse models of thyroid cancer distant metastasis developed for evaluating new therapies and studying tumor cell biology are lacking. In most transgenic mouse models of thyroid cancer, only a limited number develop spontaneous lung metastases, which are only detected *post mortem* (8–10). Several investigators have used human thyroid cancer cells stably expressing green fluorescent protein (GFP) to induce lung metastasis (11–13).

[1]Endocrine Oncology Branch, [2]Surgery Branch, and [3]Laboratory of Pathology, Center for Cancer Research, National Cancer Institute, National Institutes of Health, Bethesda, Maryland.

However, a common drawback of this approach is that the cancer's metastasis status has to be assessed at the end of the experiments by checking the isolated lungs from sacrificed mice, and thus this approach cannot be used to assess new therapies, as the tumor burden cannot be accurately assessed before treatment. CT imaging has been utilized to measure thyroid cancer lung metastasis dynamically in an orthotopic xenograft mouse model (14). However, its technical difficulty will restrict the utilization of this method. Recently, an *in vivo* detectable distant metastasis model for thyroid cancer was reported. It uses intracardiac injection of BCPAP-*luc*-IRES-GFP cells, which allows for the widespread dissemination of tumor cells and *in vivo* detection of metastatic tumors. However, intracardiac injection of tumor cells did not result in lung metastasis, the most common site of thyroid cancer metastasis (15). In this study, we report the development of a reliable and reproducible mouse model of thyroid cancer metastasis that allows sensitive, dynamic, and easy measurement of metastatic thyroid tumors in the lungs and other sites as they occur in intact animals. Such a method could accelerate the preclinical *in vivo* testing of therapeutic targets and the study of tumor cell biology.

Materials and Methods

Cell lines and animals

Human anaplastic thyroid cancer cell lines 8505C (purchased from the European Collection of Cell Cultures, Salisbury, United Kingdom), C-643 (purchased from CLS Cell Lines Service GmbH, Eppelheim, Germany), SW-1736 (purchased from CLS Cell Lines Service GmbH), THJ-16T (kindly provided by Dr. John A. Copland III, Jacksonville, FL), follicular thyroid cancer cell lines FTC-133, FTC-236, and FTC-238 (kindly provided by Dr. Peter Goretzki, Neuss, Germany), and Hürthle cell carcinoma cell line XTC-1 (kindly provided by Dr. Orlo H. Clark, San Francisco, CA) were maintained in Dulbecco's modified Eagle's medium (DMEM) supplemented with 10% fetal calf serum (FCS), penicillin (100 U/mL), streptomycin (100 μg/mL), Fungizone (250 ng/mL), thyrotropin (TSH; 10 IU/L, and insulin (10 μg/mL) in a 5% CO_2 atmosphere at 37°C. Five- to six-week-old female athymic NCr nu/nu mice were obtained from the Frederick Cancer Center Animal Facilities (Frederick National Laboratory for Cancer Research, Frederick, MD). Six- to eight-week-old NOD.Cg-*Prkdc*^{scid} *Il2rg*^{tm1Wjl}/SzJ breeder mice were purchased from The Jackson Laboratory (Bar Harbor, ME). The mice were maintained and bred according to the guidelines of the institute's Animal Advisory Committee. All the cell lines (except newly purchased C-643 and SW-1736) were authenticated by short-tandem repeat profiling on October 14, 2012, and August 30, 2013. FTC-133 has a *PTEN*-inactivating mutation and a *TP53* mutation, 8505C has *BRAF V600E* and *TP53* mutations, FTC-236 and FTC-238 have a *TP53* mutation, SW-1736 has a *BRAF V600E* mutation, C-643 has an *HRAS* mutation, and THJ-16T has *TP53*, *RB* and *PI3KCA* mutations.

Stable Luc2 *reporter cell generation*

8505C, C-643, SW-1736, THJ-16T, FTC-133, FTC-236, and FTC-238 cells were transfected with a linearized pGL4.51[*luc2*/CMV/Neo] vector (Promega, Madison, WI) encoding the luciferase reporter gene *luc2* (*Photinus pyralis*) using Lipofectamine™ 2000 reagent (Invitrogen, Carlsbad, CA). After 24 hours of transfection, cells were selected with Geneticin (600 μg/mL)-containing culture media and the G418-resistant cells were amplified in the same medium. XTC-1 cells were transduced with lentivirus baring *Luc2*-eGFP reporter genes (SAIC-Frederick, NCI-Frederick, Frederick, MD). Twenty-four hours later, cells were selected with puromycin (3 μg/mL)-containing culture medium, and the puromycin-resistant cells were amplified. The bioluminescence signal was confirmed using luciferin and the Xenogen IVIS *in vivo* imaging system (Caliper Life Sciences Inc., Hopkinton, MA). To test the correlation between bioluminescence signal intensity and cell numbers, a cell suspension with a concentration of 100,000 cells/mL was prepared and serially diluted at 1:2 until reaching a final concentration of 780 cells/mL. Cell suspensions of 100 μL of each concentration were seeded into a black 96-well plate (with a transparent bottom), then 100 μL of luciferin solution (diluted in PBS at 1 mg/mL) was added into each well. The bioluminescence signals emitted by the cells were detected 15 minutes later using the Xenogen system. The background signal from the empty wells was similar across all wells. Spearman's correlation coefficients (r) were calculated using GraphPad Prism 5 (GraphPad Software, Inc., La Jolla, CA). All experiments were performed using cells at 25 passages or fewer.

Generation of mouse models

The Animal Care and Use Committee (NCI/NIH) approved the thyroid cancer cell xenograft animal study protocol. *Luc2* reporter cells from a 70–80% confluent monolayer culture were trypsinized and suspended in DMEM. Suspensions of 3×10^4 to 7.5×10^5 cells in 0.2 mL of DMEM were injected subcutaneously into the flanks of eight-week-old nu/nu mice or intravenously through the tail veins of eight-week- to three-month-old NOD.Cg-*Prkdc*^{scid} *Il2rg*^{tm1Wjl}/SzJ mice. Immediately following implantation, bioluminescence imaging was used to assess the injected cells in all mice using the Xenogen *in vivo* imaging system. Mice were injected intraperitoneally with 3–4.5 mg of luciferin/mouse 15 minutes prior to imaging. Then the animals were anesthetized in a plastic chamber filled with a 2.5% isofluorane/oxygen/air mixture, and isofluorane anesthesia was maintained using a nose-cone delivery system during imaging. The pseudocolor image representing the spatial distribution of detected photon counts emerging from the active luciferase within each animal was collected. Signal intensity was quantified as the sum of all detected photon counts within a region of interest using IVIS Living Image software (Caliper Life Sciences Inc.). The background signal detected in the areas without xenografted cells was similar between the different mice and approximately two to three orders of magnitude lower than that of the metastasis tumor sites.

To confirm tumor development in specific organ sites, *ex vivo* images were obtained using the following method. After whole body imaging, the mice were euthanized by CO_2 inhalation, and the organs were isolated and imaged again with the Xenogen system. Then the organs were fixed in formalin for histological analysis. To identify bone

metastases, the leg and hip regions that showed strong bioluminescence signal in the whole body images were dissected out, and the skin and muscles were removed under serial Xenogen imaging. Tissue that showed a strong bioluminescence signal with a size about 8–10 mm^3 was isolated and fixed in 10% formalin.

Survival study

For animal survival analysis, two- to three-month-old NOD.Cg-*Prkdc*^{scid} *Il2rg*^{tm1Wjl}/SzJ mice were injected with 3×10^4 to 7.5×10^5 of 8505C-*Luc2* or FTC-133-*Luc2* cells through the tail vein, maintained under normal immunodeficient mouse care conditions, and monitored daily to assess their health status. Some mice were euthanized because they reached the humane euthanasia criteria endpoints (i.e., signs of severely labored breathing, rapid weight loss, hunched posture, and moribund status). At this time, they were imaged as described above, and then euthanized by CO_2 inhalation for humane reasons. In these cases, the day of euthanasia was considered the end of the survival period.

Histologic analyses

Organs and tumor xenografts were harvested, formalin-fixed, and processed into paraffin blocks for hematoxylin and eosin (H&E) staining.

Vemurafenib treatment

NOD.Cg-*Prkdc*^{scid} *Il2rg*^{tm1Wjl}/SzJ mice were injected with 8505C-*Luc2* cells (30,000 cells/mouse) into the tail vein, and lung tumor development was confirmed by imaging at one week after tumor cell implantation. Zelboraf (vemurafenib tablets; Genentech, San Francisco, CA) was grounded and suspended in 5% dextrose in 0.9% sodium chloride. Mice were gavaged with the drug suspension (100 mg/kg) or vehicle using a 20-gauge blunt-tipped gavage needle daily, starting on day 10 after tumor cell implantation until euthanization.

Statistical analysis

Kaplan–Meier survival curves and *p*-values of each pair of group comparisons were calculated using GraphPad Prism 5. The significance level was determined by using the Bonferroni method: 0.05 divided by *k* (equal to 3 in this case). If a *p*-value was smaller than this Bonferroni-corrected threshold, then the comparison was considered to be statistically significant.

Results

Generation of stably transfected Luc2 *reporter cells*

To generate stable thyroid cancer reporter cells, human anaplastic thyroid cancer cell lines 8505C, C-643, SW-1736, and THJ-16T, and follicular thyroid cancer cell lines FTC-133, FTC-236, and FTC-238 were transfected with linearized pGL4.51[*luc2*/CMV/Neo] vector encoding the luciferase reporter gene *luc2*. The Hürthle cell carcinoma cell line XTC-1 was transduced with lentivirus baring a *Luc2*-eGFP reporter gene. The stably transfected cells were selected with geneticin or puromycin respectively, and the luciferase activity was measured using luciferin and the Xenogen *in vivo* imaging system. As shown in Supplementary Figure S1 (Supplementary Data are available online at www.liebertpub.com/thy), a bioluminescent signal could be detected in fewer than 100 of the *Luc2* cells. Furthermore, the intensities of the detected signals were proportional to the numbers of seeded cells, with a correlation coefficient of about 1 for all of the cell lines (Supplementary Fig. S1).

In vivo, *noninvasive detection of thyroid cancer cells*

Since all of the reporter cell lines showed strong bioluminescent light emission *in vitro*, we next tested whether the bioluminescence intensity could be detected *in vivo* and would be proportional to the number of xenografted cells. Thus, we injected different numbers of 8505C- and FTC-133-*Luc2* cells into the tail veins of NOD.Cg-*Prkdc*^{scid} *Il2rg*^{tm1Wjl}/SzJ mice and examined the bioluminescence signals emitted by the whole mouse immediately afterward. We found that the xenografted cells quickly accumulated in the mouse lungs and emitted strong bioluminescence signals that could be easily detected when using as few as 30,000 cells (Fig. 1A).

To test whether the *in vivo* detected bioluminescence intensity was proportional to the number of xenografted tumor cells, we compared the signal intensities of the whole mouse images obtained immediately after the injections of different numbers of cells. We found that the total signal intensity detected from each individual mouse was directly proportional to the number of implanted cells (Fig. 1B, D). A similar pattern was observed for both 8505C- and FTC-133-*Luc2* cells. These results suggested that the detected bioluminescence signals could be used as an *in vivo* indicator of the numbers of xenografted tumor cells or tumor burden.

In vivo *tumor development of xenografted 8505C-*Luc2 *cells*

Injection of cancer cells via the tail vein is an established method of inducing metastatic lung tumors. To test whether we could use these *Luc2* reporter cells to generate an *in vivo* detectable thyroid cancer lung metastasis model, we injected different numbers of 8505C-*Luc2* cells into the tail veins of NOD.Cg-*Prkdc*^{scid} *Il2rg*^{tm1Wjl}/SzJ mice, and followed the tumor development by weekly monitoring of the bioluminescence signals emitted from the xenografted cells. In the first group, which received 750,000 cells per mouse, the mice showed rapid lung metastasis progression, indicated by an almost 10-fold increase in bioluminescence signals each week (Fig. 2A, B). All mice that received this number of xenografted 8505C-*Luc2* cells showed similar disease progression. Only three weeks after cancer cell injection, all treated animals had developed severe breathing difficulties, undergone rapid weight loss, and were moribund, and therefore had to be sacrificed for humane reasons. H&E staining of isolated lung tissues confirmed tumor development in the lung, with tumors occupying most of the lung (Fig. 2C).

In the second group, which received 150,000 cells per mouse, the mice also showed rapid lung tumor progression, similar to that of the first group (Fig. 2D). Some mice in the second group also developed bone metastasis (Fig. 2E). *Ex vivo* images of isolated lung and heart showed that the xenografted tumors were restricted to the lung and no tumors

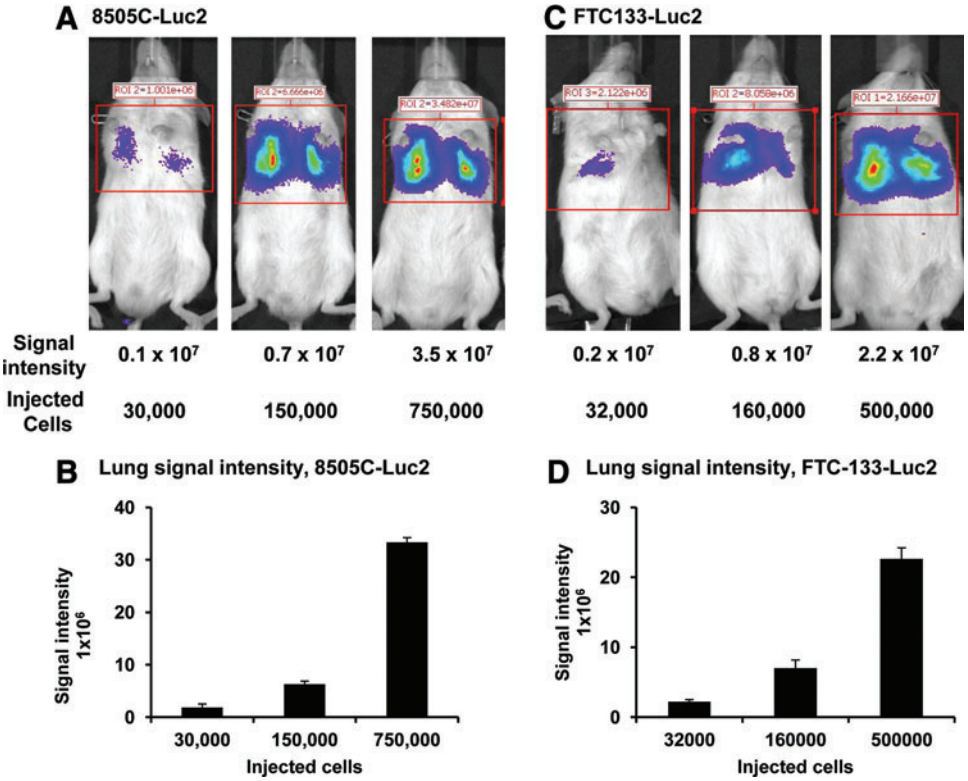

FIG 1. *In vivo* detection of *Luc2* reporter cells. The indicated number of 8505C-*Luc2* cells **(A)** and FTC-133-*Luc2* cells **(C)** were injected intravenously through the tail vein into NOD.Cg-*Prkdc*^{scid} *Il2rg*^{tm1Wjl}/SzJ mice. Bioluminescence imaging was performed immediately following implantation. The pseudocolor images represent the spatial distribution of detected photon counts emerging from active luciferase within the animals. **(B, D)** Average lung signal intensities of mice with the indicated number of injected reporter cells. $n = 3$ for each group. Error bars are standard error of the mean (SEM). Color images available online at www.liebertpub.com/thy

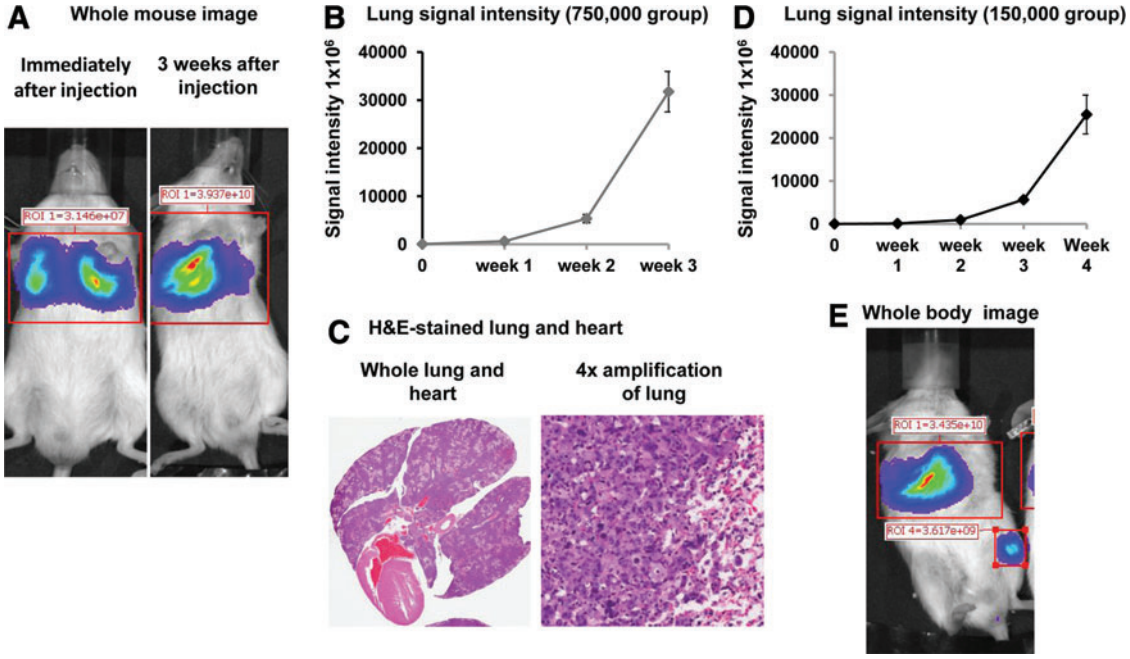

FIG 2. Lung tumor development of 8505C-*Luc2* cell injected mice. 750,000 or 150,000 cells were injected intravenously into the tail vein of NOD.Cg-*Prkdc*^{scid} *Il2rg*^{tm1Wjl}/SzJ mice. **(A)** Representative whole body images of a mouse injected with 750,000 cells taken at different times after tumor cell injection. **(B)** Average lung signal intensities of three mice injected with 750,000 cells. The measurements were performed at the indicated time points. Error bars are SEM. **(C)** Hematoxylin and eosin (H&E) staining of mouse lung and heart three weeks after tumor cell injection. **(D)** Average lung signal intensities of three mice injected with 150,000 cells. The measurements were performed at the indicated time points. Error bars are SEM. **(E)** Whole body image of mouse with bone metastasis to the hip region (150,000 cell injection). The picture was taken just before euthanasia. Color images available online at www.liebertpub.com/thy

Table 1. Rates and Sites of Thyroid Cancer Metastases

Cell line	*Cells* (n)	*Mice used* (n)	*Mice with metastasis* [n (%)]	*Mice with lung metastasis* [n (%)]
8505C[a]	30,000	39	39 (100%)	39 (100%)
	150,000	3	3 (100%)	3 (100%)
	750,000	3	3 (100%)	3 (100%)
FTC-133[a]	32,000	7	7 (100%)	6 (86%)
	160,000	7	7 (100%)	7 (100%)
	500,000	8	8 (100%)	8 (100%)
C643[b]	300,000	8	8 (100%)	8 (100%)
SW-1736[b]	300,000	7	0	0
THJ-16T[c]	300,000	7	7 (100%)	7 (100%)
XTC-1[d]	300,000	8	8 (100%)	8 (100%)
FTC-236[a]	300,000	5	5 (100%)	5 (100%)
FTC-238[a]	300,000	4	4 (100%)	4 (100%)
Total (all cell lines and all cell numbers)		106	99 (93%)	98 (92.5%)

[a]Metastasis status was examined after euthanasia.
[b]Metastasis status was examined on the 7th week after cell injection.
[c]Metastasis status was examined on the 4th week after cell injection.
[d]Metastasis status was examined on the 6th week after cell injection.

were observed in the heart, which was confirmed by H&E staining of the tissues (data not shown).

In the third group, only 30,000 8505C-*Luc2* cells were injected into each mouse. Even though the number of xenografted cells was very low, every mouse in this group developed lung tumors (Table 1). In addition, some of the mice developed bone tumors, though at a later stage (five to six weeks after injection), and they were all located in the hip region (Fig. 3A–C and Supplementary Table S1). The bioluminescence signals emitted from the bone tumors were about 1×10^9 to 5×10^9.

To assess the disease progression rate, some mice that received different numbers of 8505C-*Luc2* cell injections were followed. Compared to the mice that received higher numbers of cells, the disease progression of the mice injected with 30,000 cells was slower. The mice in this group had a survival time of 35–46 days after tumor cell injection (Fig. 3D).

In vivo *tumor development of xenografted FTC-133*-Luc2 *cells*

To test the metastatic tumor development of FTC-133-*Luc2* cells, 32,000–500,000 cells were injected into the tail veins of NOD.Cg-*Prkdc*^{scid} *Il2rg*^{tm1Wjl}/SzJ mice, and tumor development was followed by monitoring the bioluminescence signals weekly. All of the mice developed metastatic tumors. Among these mice, 21/22 had lung metastases, and 9/22 mice also developed liver metastases (Fig. 4A–C, Table 1, and Supplementary Table S1). Generally, disease progression was faster in the mice that were injected with more FTC-133-*Luc2* cells than in those injected with fewer (Fig. 4D).

In vivo *tumor development of xenografted FTC-236*-Luc2, *FTC-238*-Luc2, *C-643*-Luc2, *SW-1736*-Luc2, *THJ-16T*-Luc2, *and XTC-1*-Luc2 *cells*

To test whether the *in vivo* detectable metastatic tumor could also be developed by using other *Luc2* reporter cells, 300,000 of FTC-236-*Luc2*, FTC-238-*Luc2*, C-643-*Luc2*, *SW-1736-Luc2, THJ-16T-Luc2*, and *XTC-1-Luc2* cells were injected into the tail veins of NOD.Cg-*Prkdc*^{scid} *Il2rg*^{tm1Wjl}/SzJ mice and tumor development followed by monitoring the bioluminescence signals weekly. All cell lines except SW-1736-*Luc2* cells developed detectable metastatic tumors (Table 1 and Supplementary Table S1).

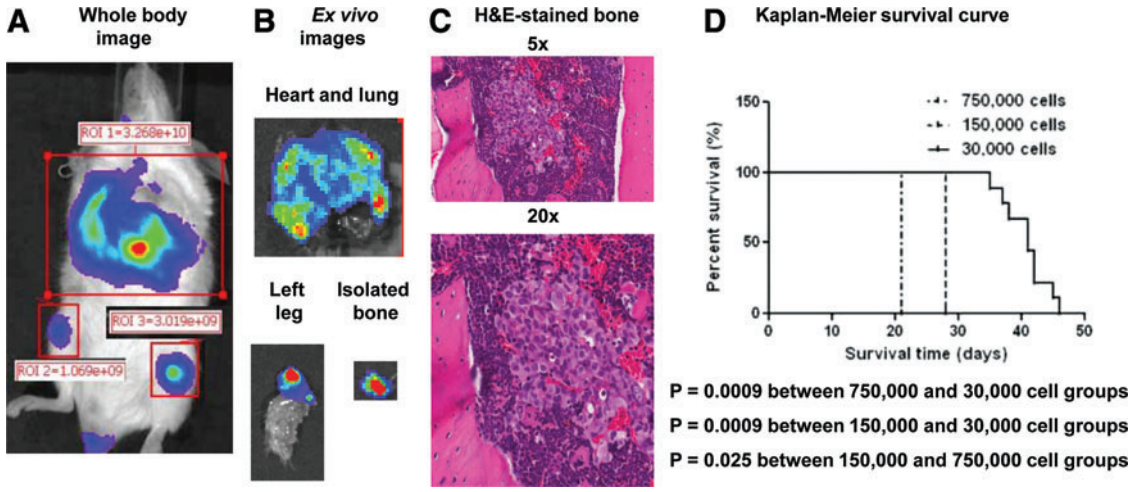

FIG 3. Tumor development in mice injected with 30,000 8505C-*Luc2* cells. **(A)** Representative whole body image of a mouse immediately before euthanasia. **(B)** *Ex vivo* images of mouse heart, lung, leg, and isolated bone. **(C)** H&E staining of a mouse bone metastasis. **(D)** Kaplan–Meier survival curve of mice according to the number of injected 8505C-*Luc2* cells. $n=3$ for the 750,000 and 150,000 cell groups, and $n=8$ for the 30,000 cell group. Color images available online at www.liebertpub.com/thy

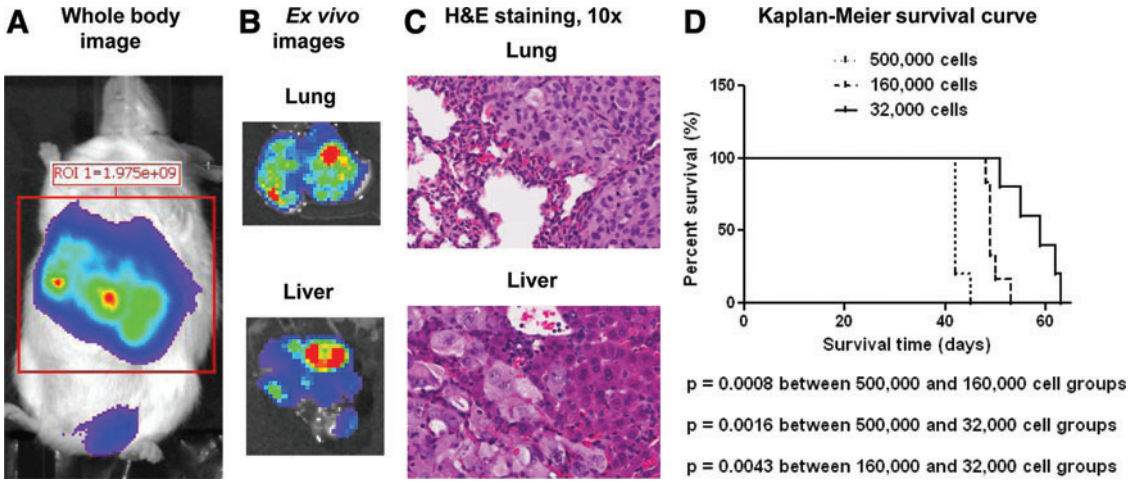

FIG 4. Tumor development in mice injected with FTC-133-*Luc2* cells. **(A)** Representative whole body image of a mouse immediately before euthanization. **(B)** *Ex vivo* images of mouse lung and liver. **(C)** H&E staining of mouse lung and liver metastasis tumors. **(D)** Kaplan–Meier survival curve of mice according to the number of FTC-133-*Luc2* cells injected. $n=5$ for the 500,000 cell group, $n=6$ for the 160,000 cell group, and $n=5$ for the 32,000 cell group. Color images available online at www.liebertpub.com/thy

In vivo *bioluminescence intensity is an indicator of mouse tumor burdens*

To test whether the *in vivo* bioluminescence intensity could be used as an accurate measure of tumor burden or size, we injected 8505C-*Luc2* and FTC-133-*Luc2* cells subcutaneously into the flanks of nu/nu mice, waited for tumor development, and then compared the tumor's sizes to the bioluminescence signals emitted. As shown in Figure 5, the signal intensities detected from these tumors were directly proportional to the sizes of the tumors ($r=0.98$ for 8505C-*Luc2* tumors; $r=0.94$ for FTC-133-*Luc2* tumors).

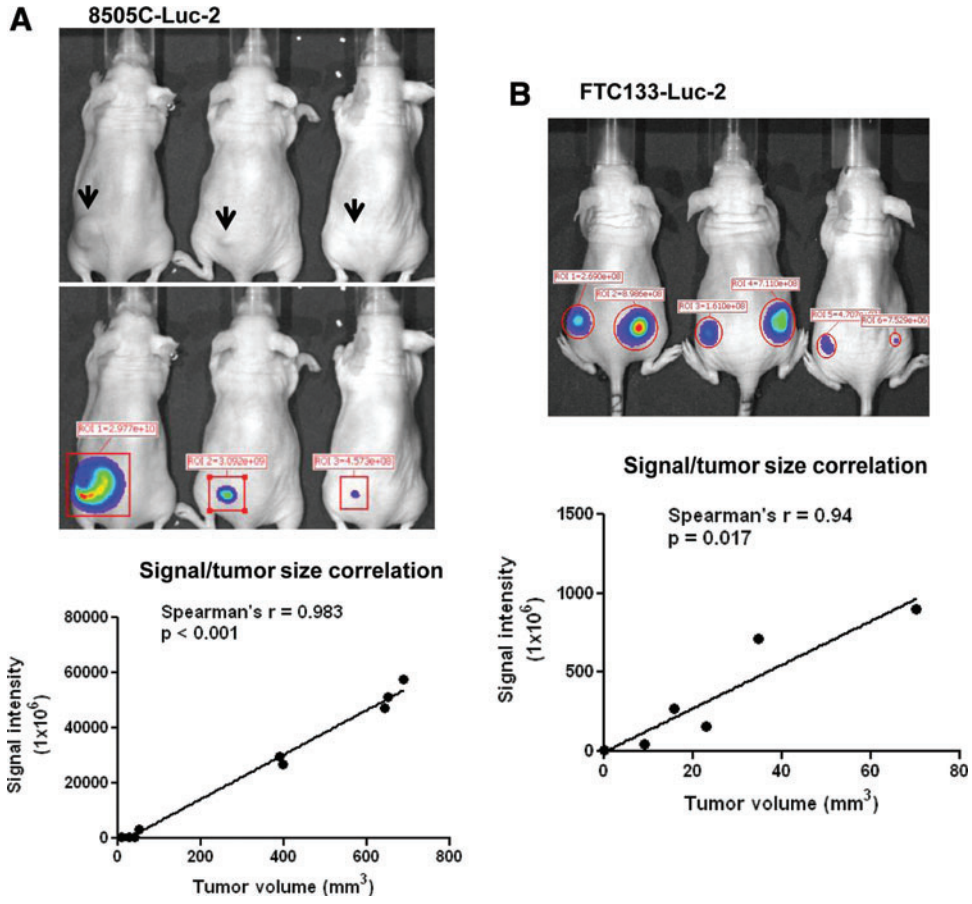

FIG 5. *In vivo* bioluminescence intensity correlates with xenograft tumor size. **(A)** Representative image of nu/nu mice with subcutaneous tumors generated from 8505C-*Luc2* cells, and the correlation of signal intensity versus tumor volume (tumor number = 9). **(B)** nu/nu mice with subcutaenous tumors generated from FTC-133-*Luc2* cells, and the correlation of signal intensity versus tumor volume (tumor number = 6). Color images available online at www.liebertpub.com/thy

We also tested whether the *in vivo* bioluminescence measurement could be used as an indicator of the tumor burden of internal organs. To do this, we injected 30,000 8505C-*Luc2* cells into the tail veins of NOD.Cg-*Prkdc*^{scid} *Il2rg*^{tm1Wjl}/SzJ mice, followed the tumor development by monitoring the bioluminescence signals, and euthanized the animals at different time intervals. The tumor burden in the lung was evaluated by weighing the isolated lung, performing H&E staining on it, and comparing the stained images with the *in vivo* bioluminescence images taken just before euthanization (Supplementary Fig. S2). As shown in Figure 6, the *in vivo* detected bioluminescence signals directly reflected the tumor burdens of the lungs.

Monitoring of response to vemurafenib treatment in in vivo *metastasis model generated with 8505C-*luc2 *BRAF V600E mutant cells*

Vemurafenib, a BRAF inhibitor, was used to treat lung metastases generated from 8505C-*Luc2* BRAF V600E mutation cells to test the accuracy of the model to evaluate response to therapy. After the confirmation of lung tumor development by *in vivo* imaging, the mice were randomized into two groups, and received vemurafenib or vehicle treatment through oral gavage. Tumor progressions in the mice were monitored weekly by imaging. As shown in Figure 7A, control mice showed rapid tumor growth indicated by the dramatic increase in the bioluminescence signals. After one

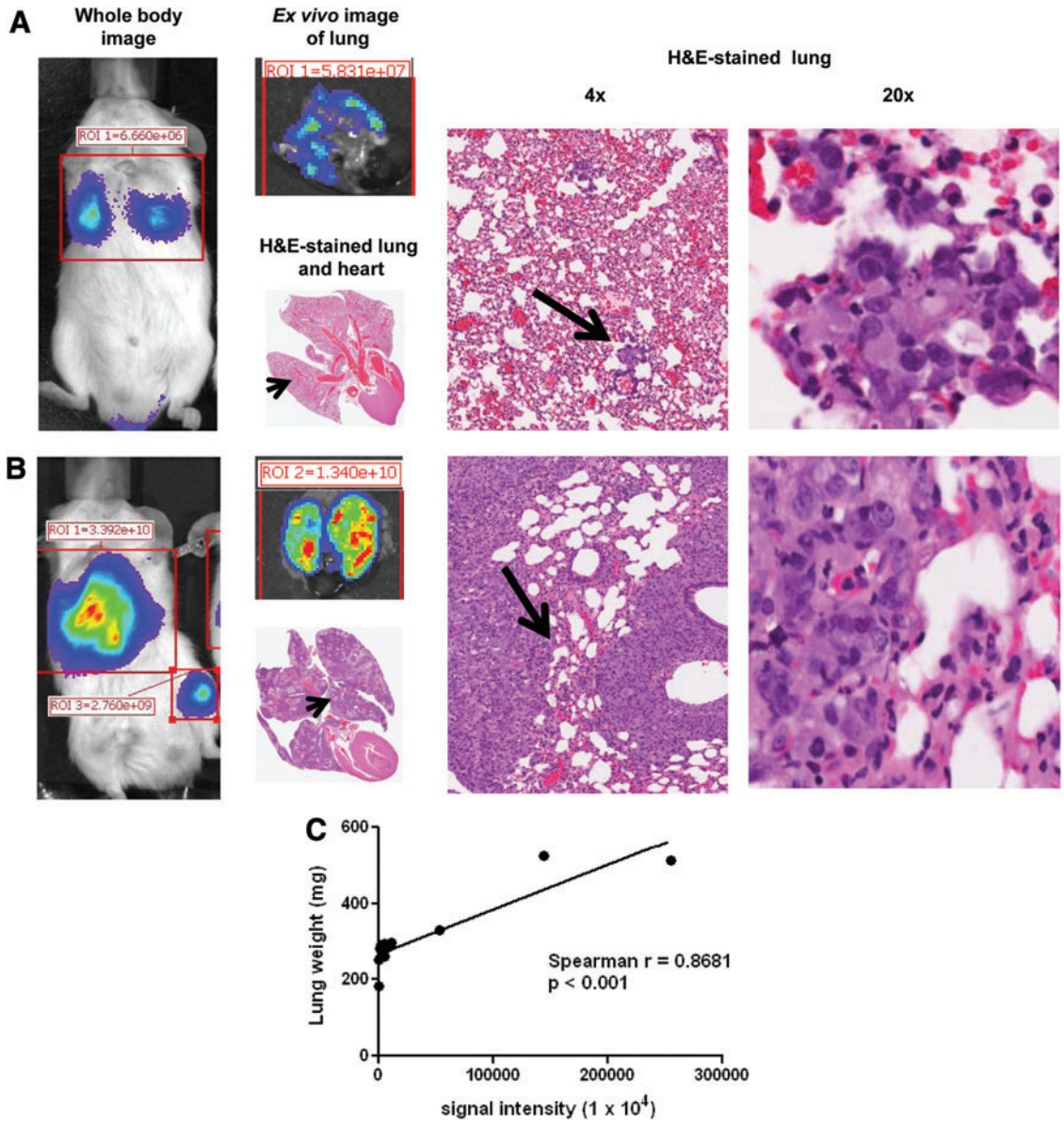

FIG 6. *In vivo* bioluminescence intensity correlates with the mouse xenograft tumor burden. **(A, B)** 30,000 8505C-*Luc2* cells were injected into the tail vein and the mice euthanized two weeks **(A)** and five weeks **(B)** after injection. Shown are representative whole body and lung images, and H&E-stained lung sections. **(C)** Relationship between lung bioluminescence signal intensity (taken just before euthanasia) and the weight of the isolated lung. $n = 13$. Color images available online at www.liebertpub.com/thy

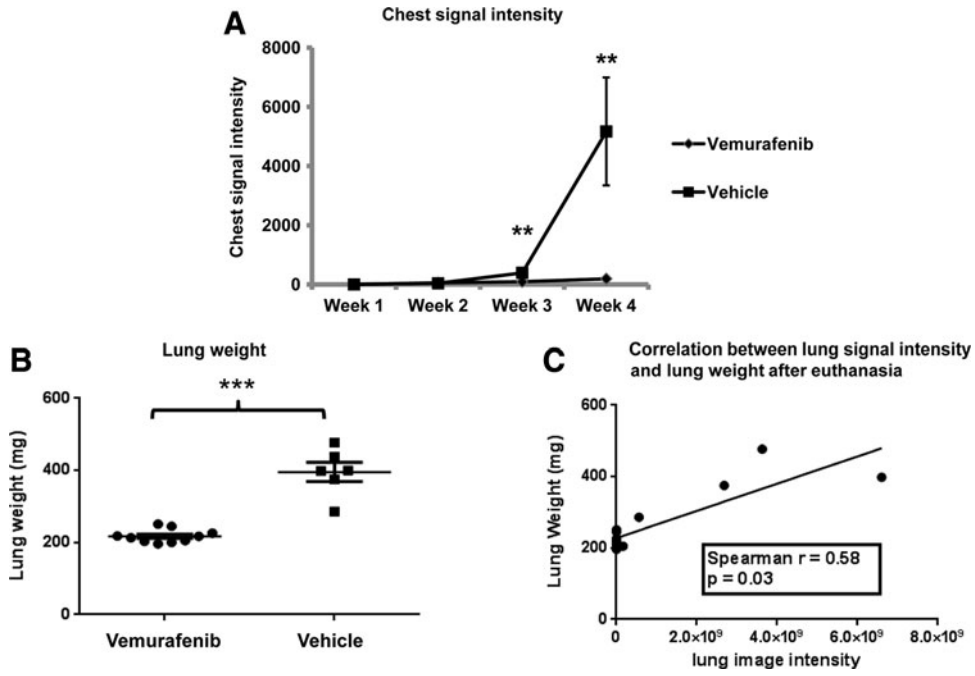

FIG 7. Monitoring response to therapy in *in vivo* mouse model of metastasis. **(A)** Mouse lung bioluminescence signal intensities measured at the indicated time points (normalized to the initial imaging before treatment) with and without vemurafenib treatment in the mice injected with 8505C-*Luc2 BRAF* V600E mutant cells. **(B)** Weights of isolated lungs after euthanasia in vemurafenib treated and untreated groups. **(C)** Relationship between lung bioluminescence signal intensity and the isolated lung weight at euthanasia ($n = 14$). 8505C-*Luc2* BRAF *V600E* mutant cells were injected into NOD.Cg-*Prkdc*^{scid} *Il2rg*^{tm1Wjl}/SzJ mice (30,000 cells/mouse) tail veins, and tumor metastasis development confirmed by *in vivo* imaging one week after injection. On the 10th day after injection of cells, mice were divided into two groups (control group and vemurafenib group, $n = 16$) and treated with vemurafenib or vehicle daily.

month, all mice in the vehicle control group started to show breathing difficulty and rapid weight loss, and were euthanized by 38–42 days after tumor implantation. As expected, vemurafenib-treated mice showed much slower tumor progression (Fig. 7A). To compare the lung tumor status between the two groups, vemurafenib-treated mice were also euthanized at 42 days after tumor implantation (the day that the last control mouse was euthanized), and their lungs were isolated, weighed, and compared to that of the control group. As shown in Figure 7B and C, the lung weights of control mice were significantly higher compared to that of vemurafenib-treated mice, and there was a good correlation between the signal intensity and actual lung tumor weight at euthanization, indicating the *in vivo* bioluminescence signal accurately reflects the tumor response to vemurafenib treatment.

Discussion

The present study was designed to develop a mouse model for metastatic thyroid cancer that would be reliable and reproducible, and allow for easy, noninvasive detection of tumor burdens. To achieve this, we generated stable luciferase reporter cell lines in anaplastic thyroid cancer cell lines (8505C, C-643, SW-1736, and THJ-16T), follicular thyroid cancer cell lines (FTC-133, FTC-236, and FTC-238), and a Hürthle cell carcinoma cell line (XTC-1). With their high signal intensity and low background, these reporter cells could be easily detected *in vivo*. Following tail vein injection, mice bearing as few as 30,000 8505C-*Luc2* cells quickly developed *in vivo* measurable lung metastases, and some of these mice also developed bone tumor(s) at a later stage of the disease. We also demonstrate an excellent correlation between bioluminescence signal intensity and tumor burden *in vivo* in flank and lung metastasis xenografts. To our knowledge, this is the first thyroid cancer lung metastasis model with a high metastasis take rate, and that allows easy, noninvasive, and dynamic tumor development follow-up, which could be used for preclinical evaluation of new therapies and to study tumor cell biology.

Anaplastic thyroid cancer is a rare but lethal disease, with a mean survival of six months from diagnosis (6). While differentiated thyroid cancer generally has a favorable prognosis, many patients have significant morbidity and mortality due to distant metastasis. The most common metastasis site for thyroid cancer is the lung, followed by bone (2). Thus far, there have been no effective treatment approaches for patients with metastatic thyroid cancers who are not responsive to conventional therapy, and neither chemotherapy nor radiation therapy are effective at prolonging survival in patients with anaplastic thyroid cancer (16). Therefore, alternative systemic treatments are needed, but they need to be tested in *in vivo* models that recapitulate the burden and site of the disease that causes the most morbidity and mortality.

We used NOD.Cg-*Prkdc*^{scid} *Il2rg*^{tm1Wjl}/SzJ mice in our studies for several important reasons. First, metastasis engraftment rates are higher in these mice than in *Foxn1nu* (nude) mice, most likely due to their immunologic background (17,18). NOD.Cg-*Prkdc*^{scid} *Il2rg*^{tm1Wjl}/SzJ mice have the combined features of the NOD/ShiLTJ background severe combined immune deficiency mutation [SCID] and the

IL2 receptor gamma chain deficiency. Thus, these mice do not have B-cells, mature T-cells, or functional natural killer cells, and lack cytokine signaling, leading to better engraftment of human stem cells and peripheral mononuclear cells than any other mouse strain currently being used (19). Second, because cost is an important consideration when performing *in vivo* studies, the NOD.Cg-*Prkdc*^{scid} *Il2rg*^{tm1Wjl}/SzJ mice, unlike nude mice, can be easily bred for such studies. In fact, all the mice we used in our studies were generated from nine breeder mice (six females and three males).

To test new therapies, several mouse models of human thyroid cancers have been developed, including xenograft, orthotopic, and transgenic or genetically engineered mice (9,10,13,15,20–23). The most commonly used animal model in drug testing is subcutaneous implantation of human thyroid cancer cells into immunocompromised mice. It is easy to perform, easy to monitor the tumor growth, and easy to follow up the treatment response by using caliper measurements. However, this model may not be representative of metastatic thyroid cancer biology as the microenvironment of the xenografted tumor's subcutaneous implantation site and that of human cancer metastases in organs, such as lung and bone, are very different. In fact, it has been reported that subcutaneous implantation of 8505C cells resulted in much smaller tumors compared to orthotopic placement of the same cells (21). Several studies have suggested that the phenotypes of cancer cells can be modulated via their interaction with surrounding tissues, and therapy responses can be very different between subcutaneous tumors and lung metastases (24,25). We have also observed that subcutaneous injection of 8505C cells into the flanks of nude mice results in much slower tumor growth than that observed in the follicular cancer cell line FTC-133, which is in contrast to their typical aggressive growth in humans. However, in our current lung metastasis model, the progression rates of lung tumors generated by these two cell lines and the xenografted mouse survival rates were reversed to mimic the natural features of these cell lines. Therefore, in contrast to models using subcutaneous xenografted tumors, the lung and bone thyroid cancer metastasis model may better reproduce the tumor microenvironment and better predict treatment responses to new therapies. Xenografted lung metastasis thyroid cancer models have been previously reported (20). However, their metastasis rates are low and, due to the lack of an *in vivo* tumor detection method, a common drawback of these models is that the tumor metastasis status can only be assessed by checking the isolated organs at the end of experiment, which is time consuming and potentially inaccurate. Also, such approaches for evaluating new experimental therapies require sacrificing the animal and do not allow evaluation of the natural history of the disease after treatment withdrawal in cases where tumor regression is observed. Similarly, experiments using transgenic or genetically engineered thyroid cancer mouse models face the same problems. In contrast, our model, as demonstrated by the vemurafenib treatment experiment (Fig. 7), with its high sensitivity and low background levels, allows the easy assessment of metastatic tumors in the whole animal and, even more important, allows a dynamic follow-up of metastatic tumor development when studying the effect of experimental therapies or tumor cell biology. As previously mentioned, the novel metastatic thyroid cancer model reported in this study is technically easy and reproducible. Therefore, it might serve as an effective tool in preclinical studies of new therapies for metastatic anaplastic and differentiated thyroid cancer. In addition, this model also will serve as an important tool for *in vivo* studies of thyroid cancer tumor biology.

Acknowledgments

We thank Dr. Bih-Rong Wei (NCI/NIH) and Dr. Yaroslav Teper (NCI/NIH) for technical help. This research was supported by the Intramural Research Program, Center for Cancer Research, National Cancer Institute, National Institutes of Health.

Author Disclosure Statement

No competing financial interests exist for any author.

References

1. Howlader N NA, Krapcho M, Neyman N, Aminou R, Waldron W, Altekruse SF, Kosary CL, Ruhl J, Tatalovich Z, Cho H, Mariotto A, Eisner MP, Lewis DR, Chen HS, Feuer EJ, Cronin KA, Edwards BK (eds) 2011 SEER Cancer Statistics Review, 1975–2008. National Cancer Institute, Bethesda, MD, based on November 2010 SEER data submission, posted to the SEER Web site. http://seer.cancer.gov/archive/csr/1975_2008/
2. Ruegemer JJ, Hay ID, Bergstralh EJ, Ryan JJ, Offord KP, Gorman CA 1988 Distant metastases in differentiated thyroid carcinoma: a multivariate analysis of prognostic variables. J Clin Endocrinol Metab **67:**501–508.
3. Shaha AR 2012 Recurrent differentiated thyroid cancer. Endocr Pract **18:**600–603.
4. Clark OH 1996 Predictors of thyroid tumor aggressiveness. West J Med **165:**131–138.
5. Hundahl SA, Fleming ID, Fremgen AM, Menck HR 1998 A National Cancer Data Base report on 53,856 cases of thyroid carcinoma treated in the U.S., 1985–1995 [see comments]. Cancer **83:**2638–2648.
6. Smallridge RC, Copland JA 2010 Anaplastic thyroid carcinoma: pathogenesis and emerging therapies. Clin Oncol (R Coll Radiol) **22:**486–497.
7. McIver B, Hay ID, Giuffrida DF, Dvorak CE, Grant CS, Thompson GB, van Heerden JA, Goellner JR 2001 Anaplastic thyroid carcinoma: a 50-year experience at a single institution. Surgery **130:**1028–1034.
8. Zhu XG, Zhao L, Willingham MC, Cheng SY 2010 Thyroid hormone receptors are tumor suppressors in a mouse model of metastatic follicular thyroid carcinoma. Oncogene **29:**1909–1919.
9. Knostman KA, Jhiang SM, Capen CC 2007 Genetic alterations in thyroid cancer: the role of mouse models. Vet Pathol **44:**1–14.
10. Kim WG, Guigon CJ, Fozzatti L, Park JW, Lu C, Willingham MC, Cheng SY 2012 SKI-606, an Src inhibitor, reduces tumor growth, invasion, and distant metastasis in a mouse model of thyroid cancer. Clin Cancer Res **18:**1281–1290.
11. Nucera C, Porrello A, Antonello ZA, Mekel M, Nehs MA, Giordano TJ, Gerald D, Benjamin LE, Priolo C, Puxeddu E, Finn S, Jarzab B, Hodin RA, Pontecorvi A, Nose V, Lawler J, Parangi S 2010 B-Raf(V600E) and thrombospondin-1 promote thyroid cancer progression. Proc Natl Acad Sci USA **107:**10649–10654.

12. Burrows N, Babur M, Resch J, Ridsdale S, Mejin M, Rowling EJ, Brabant G, Williams KJ 2011 GDC-0941 inhibits metastatic characteristics of thyroid carcinomas by targeting both the phosphoinositide-3 kinase (PI3K) and hypoxia-inducible factor-1alpha (HIF-1alpha) pathways. J Clin Endocrinol Metab **96:**E1934–E1943.
13. Nehs MA, Nucera C, Nagarkatti SS, Sadow PM, Morales-Garcia D, Hodin RA, Parangi S 2012 Late intervention with anti-BRAF(V600E) therapy induces tumor regression in an orthotopic mouse model of human anaplastic thyroid cancer. Endocrinology **153:**985–994.
14. Liu W, Cheng S, Asa SL, Ezzat S 2008 The melanoma-associated antigen A3 mediates fibronectin-controlled cancer progression and metastasis. Cancer Res **68:**8104–8112.
15. Chan CM, Jing X, Pike LA, Zhou Q, Lim DJ, Sams SB, Lund GS, Sharma V, Haugen BR, Schweppe RE 2012 Targeted inhibition of Src kinase with dasatinib blocks thyroid cancer growth and metastasis. Clin Cancer Res **18:**3580–3591.
16. Cooper DS, Doherty GM, Haugen BR, Kloos RT, Lee SL, Mandel SJ, Mazzaferri EL, McIver B, Sherman SI, Tuttle RM 2006 Management guidelines for patients with thyroid nodules and differentiated thyroid cancer. Thyroid **16:**109–142.
17. Giordano Attianese GM, Marin V, Hoyos V, Savoldo B, Pizzitola I, Tettamanti S, Agostoni V, Parma M, Ponzoni M, Bertilaccio MT, Ghia P, Biondi A, Dotti G, Biagi E 2011 In vitro and in vivo model of a novel immunotherapy approach for chronic lymphocytic leukemia by anti-CD23 chimeric antigen receptor. Blood **117:**4736–4745.
18. Teraoka S, Kyoizumi S, Seyama T, Yamakido M, Akiyama M 1994 Scid mice model for the in-vivo study of human oncotherapy—studies on the growth and metastasis of human lung-cancer. Int J Oncol **5:**501–508.
19. Shultz LD, Lyons BL, Burzenski LM, Gott B, Chen X, Chaleff S, Kotb M, Gillies SD, King M, Mangada J, Greiner DL, Handgretinger R 2005 Human lymphoid and myeloid cell development in NOD/LtSz-scid IL2R gamma null mice engrafted with mobilized human hemopoietic stem cells. J Immunol **174:**6477–6489.
20. Hoelting T, Goretzki PE, Duh QY 2001 Follicular thyroid cancer cells: a model of metastatic tumor in vitro (review). Oncol Rep **8:**3–8.
21. Nucera C, Nehs MA, Mekel M, Zhang X, Hodin R, Lawler J, Nose V, Parangi S 2009 A novel orthotopic mouse model of human anaplastic thyroid carcinoma. Thyroid **19:**1077–1084.
22. Younes MN, Yigitbasi OG, Park YW, Kim SJ, Jasser SA, Hawthorne VS, Yazici YD, Mandal M, Bekele BN, Bucana CD, Fidler IJ, Myers JN 2005 Antivascular therapy of human follicular thyroid cancer experimental bone metastasis by blockade of epidermal growth factor receptor and vascular growth factor receptor phosphorylation. Cancer Res **65:**4716–4727.
23. Ahn SH, Henderson Y, Kang Y, Chattopadhyay C, Holton P, Wang M, Briggs K, Clayman GL 2008 An orthotopic model of papillary thyroid carcinoma in athymic nude mice. Arch Otolaryngol Head Neck Surg **134:**190–197.
24. Fidler IJ, Wilmanns C, Staroselsky A, Radinsky R, Dong Z, Fan D 1994 Modulation of tumor cell response to chemotherapy by the organ environment. Cancer Metastasis Rev **13:**209–222.
25. Dong Z, Radinsky R, Fan D, Tsan R, Bucana CD, Wilmanns C, Fidler IJ 1994 Organ-specific modulation of steady-state mdr gene expression and drug resistance in murine colon cancer cells. J Natl Cancer Inst **86:**913–920.

Address correspondence to:
Electron Kebebew, MD
Endocrine Oncology Branch
National Cancer Institute
10 Center Drive, MSC 1201
Bethesda, MD 20892-1201

E-mail: kebebewe@mail.nih.gov